

Cross-correlation of Cosmic Infrared Background Anisotropies with Large Scale Structures[★]

P. Serra¹, G. Lagache¹, O. Doré^{2,3}, A. Pullen^{2,3}, and M. White^{4,5}

¹ Institut d'Astrophysique Spatiale (IAS), Bâtiment 121, F- 91405 Orsay (France); Université Paris-Sud 11 and CNRS (UMR 8617)
e-mail : pserra@ias.u-psud.fr

² Jet Propulsion Laboratory, California Institute of Technology, 4800 Oak Grove Drive, Pasadena, California, U.S.A.

³ California Institute of Technology, Pasadena, California, U.S.A.

⁴ Department of Physics, University of California Berkeley, CA 94720, USA

⁵ Lawrence Berkeley National Laboratory, 1 Cyclotron Rd, Berkeley, CA 94720, USA

Received ? / Accepted ?

ABSTRACT

We measure the cross-power spectra between Luminous Red Galaxies (LRGs) from SDSS-III Data Release Eight (DR8) and Cosmic Infrared Background (CIB) anisotropies from *Planck* and IRIS at 353, 545, 857 and 3000 GHz (corresponding to 850, 550, 350 and 100 μm , respectively) in the multipole range $100 < l < 1000$. Using approximately $6.5 \cdot 10^5$ photometrically determined LRGs in 7760 deg^2 of the Northern Hemisphere in the redshift range $0.45 < z < 0.65$, and modeling the CIB anisotropies with an extended version of the halo model, we confirm the basic picture obtained from recent analyses of CIB anisotropies with *Herschel* and *Planck* that the most efficient halo mass at hosting star forming galaxies is $\log(M_{\text{eff}}/M_{\odot}) = 12.84 \pm 0.15$. We also estimate the percentage of CIB anisotropies correlated with LRGs as approximately 11.8%, 3.9%, 1.8% and 1.0% of the total at 3000, 857, 545 and 353 GHz, respectively. At redshift $z \sim 0.55$, the bias of CIB galaxies with respect to the dark-matter density field has the value $b_{\text{CIB}} \sim 1.45$, and mean dust temperature of CIB galaxies is $T_d = 26$ K.

Key words. Galaxies: star formation - Galaxies: statistics - Galaxies: halos - Dark Matter - Infrared: galaxies

1. Introduction

The Cosmic Infrared Background (CIB), detected with both FIRAS (Puget et al. 1996; Fixsen et al. 1998; Lagache et al. 1999) and DIRBE (Hauser et al. 1998; Lagache et al. 2000), is due to thermal emission from warm dust enshrouding star-forming regions in galaxies. Spatial CIB fluctuations were discovered by the Spitzer Space Telescope (Lagache et al. 2007), the BLAST balloon experiment (Viero et al. 2009) and the Herschel Space Observatory (Amblard et al. 2011); in the same period, different CMB experiments extended these detections to longer wavelengths (Hall et al. 2010; Dunkley et al. 2011; Reichardt et al. 2012). The *Planck* early results paper Planck Collaboration XVIII 2011 measured angular power spectra of CIB anisotropies from arc-minute to degree scales at 217, 353, 545 and 857 GHz and the recent paper Planck Collaboration XXX 2013 represents its extension and improvement in terms of analysis and interpretation, establishing *Planck* as a powerful probe of the CIB clustering. The sources making up the CIB are thought to trace the underlying dark-matter field and this implies a certain degree of correlation with any other tracer of the dark-matter distribution, provided that both tracers have overlapping redshifts. A useful property of such cross-correlation studies is that the measurement can be used to isolate and analyze a small redshift range in one signal (e.g. the CIB) if the other population is

limited in redshift (e.g. the LRGs). In addition, the measurement is not prone to systematics that are not correlated between the two datasets, giving thus a strong signal even if each dataset is contaminated by other physical effects. As shown in Planck Collaboration XXX (2013) for example, foreground Galactic dust severely limits CIB measurements at the high frequency channels ($\nu \geq 545$ GHz) while Cosmic Microwave Background (CMB) anisotropies contaminate the CIB signal at frequencies $\nu \leq 353$ GHz; possible approaches to dealing with these foregrounds include their inclusion in the likelihood analysis (e.g., as a power law) or their removal using a tracer of dust and possibly selecting very clean regions of the sky. In any event, the presence of foreground and background contamination greatly complicates the analysis of CIB data. This limitation disappears when cross-correlating CIB maps with catalogs of dark matter tracers not directly correlated with Galactic dust or CMB (e.g., Planck Collaboration XVIII 2013); in this case the presence of uncorrelated contaminants only appears in the computation of the uncertainties associated to the measurement. In this paper we perform a measurement of the cross-correlation between CIB maps from *Planck* and IRIS and a galaxy map of Luminous Red Galaxies (LRG) from SDSS-III Data Release 8 (DR8). Fixing both the LRG redshift distribution and their bias with respect to the dark-matter field, we will be able to constrain the mean value of the dark-matter halo mass which is most efficient at hosting star formation.

A measurement of the cross-correlation between CIB sources and other tracers of the dark-matter field at high redshift can be extremely important in constraining the early star-formation

[★] Based on observations obtained with *Planck* (<http://www.esa.int/Planck>), an ESA science mission with instruments and contributions directly funded by ESA Member States, NASA, and Canada.

history of the Universe and the clustering properties of high-redshift objects. In this regard, it is important to keep in mind that a good knowledge of the redshift distribution of the sources to be cross-correlated with the CIB is mandatory in order to constrain both the CIB emissivity and the bias of both tracers. The quasars catalog from WISE (Wright et al. 2010) (whose redshift distribution can be inferred using the method developed in e.g., Ménard et al. (2013)), and the spectroscopic quasars from BOSS (Pâris et al. 2013) will certainly be important for such studies. However, our quite thorough attempt at computing their cross-power spectrum with the CIB maps has shown the existence of possible systematics that have not been well understood. In particular, when cross-correlating with the spectroscopic BOSS quasar catalog, we find a strong anti-correlation at large angular scales whose origin, among many possibilities, has not been clearly isolated. On the other hand, the difficulty in selecting objects in the WISE dataset (beyond the approximate method based on color cuts explained in Wright et al. (2010)), does not allow to clearly interpret the results of the cross-correlation in the context of the halo model. We thus decided not to include these datasets in the present analysis and to defer this kind of study to a future publication.

Throughout this paper, we adopt the standard flat Λ CDM cosmological model as our fiducial background cosmology, with parameter values derived from the best-fit model of the CMB power spectrum measured by *Planck* Planck Collaboration XVI 2013: $\{\Omega_m, \Omega_\Lambda, \Omega_b h^2, \sigma_8, h, n_s\} = \{0.3175, 0.6825, 0.022068, 0.8344, 0.6711, 0.9624\}$. We also define halos as matter overdense regions with a mean density equal to 200 times the mean density of the Universe, and we assume a Navarro-Frenck-White (NFW) profile (Navarro et al. 1997) with a concentration parameter as in Cooray & Sheth (2002). The fitting function of Tinker et al. (2008) is used for the halo-mass function while sub-halo mass function and halo bias are taken as in Tinker et al. (2010).

2. Data

2.1. CMASS catalog

The publicly available SDSS-III DR8 catalog¹ (Eisenstein et al. 2011; Ross et al. 2011; Ho et al. 2012; de Putter et al. 2012) consists of LRGs with photometric redshift in the range $0.45 < z_{phot} < 0.65$, centered around $\bar{z} = 0.55$ (see Fig 2), and selected with the same color and magnitude cuts as the SDSS-III "CMASS" (constant mass) sample from BOSS (White et al. 2011; Ho et al. 2012). In order to create a galaxy map from the catalog, we use the HEALPix² pixelization scheme of the sphere (Górski et al. 2005) at resolution $N_{side} = 1024$; objects are weighted with their probability of being a galaxy and pixelized as number overdensities δ_i with respect to the mean number of galaxies \bar{n} in each pixel, as:

$$\delta_i \equiv (n_i - \bar{n})/\bar{n}. \quad (1)$$

In order to reduce systematic effects due to complicated mask geometries, we use only data in the Northern hemisphere, with the same footprint as in Thomas et al. (2011); this choice reduces the total area available of approximately 1300 deg^2 , leaving 7760 deg^2 with approximately 650,000 galaxies, but ensures stability

¹ <http://portal.nersc.gov/project/boss/galaxy/photoz/>

² <http://healpix.jpl.nasa.gov/>

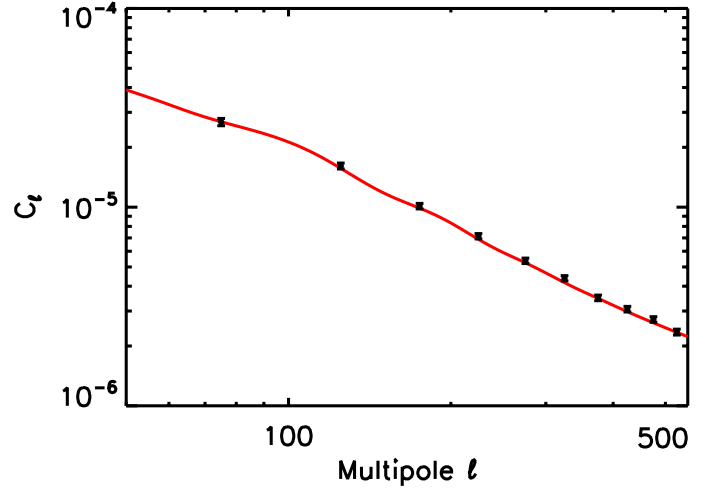


Fig. 1. Angular auto-power spectrum measured in the SDSS-III DR8 LRG survey

of results, as shown in the Appendix A, where we confront error bars computed analytically with those estimated from Monte Carlo simulations. An accurate analysis of potential systematics affecting our dataset, stressing the contribution of seeing effects, sky brightness and stellar contamination, has been performed in Ross et al. (2011) and Ho et al. (2012), and we will shape our galaxy mask according to their prescriptions to reduce these effects.

As shown in Fig. 1, the computation of the LRG auto-power spectrum from these data is compatible with a non-linear prescription for the dark matter power spectrum (we used the Halofit routine (Smith et al. 2003) in CAMB³), together with a scale and redshift independent galaxy bias parameter $b_{LRG} = 2.1 \pm 0.02$, in agreement with Ross et al. (2011), and with a galaxy redshift distribution centered in $\bar{z} = 0.55$ and with spread $\sigma = 0.07$:

$$\frac{dN}{dz}|_{LRG} \propto \exp(-(z - \bar{z})^2 / (2\sigma^2)), \quad (2)$$

as shown in Fig. 2.

In the rest of our analysis we use Eq. 2 to compute the LRG redshift distribution, and we fix the LRG bias to the value $b_{LRG} = 2.1$.

2.2. Planck and IRIS maps

We use intensity maps at 353, 545 and 857 GHz from the public data release of the first 15.5 months of *Planck* operations Planck Collaboration I 2013, together with a far-infrared map at 3000 GHz from IRAS (IRIS, Miville-Deschênes et al. 2002; Miville-Deschênes & Lagache 2005). We do not use the lower frequency *Planck* channels in our analysis, as they contain a large contribution from primary CMB anisotropies and, for the redshift distribution of the galaxy sample considered here, most of the cross-correlation signal comes from the higher frequency maps. Finally, the large number of point sources to be masked in the IRAS 3000 GHz map creates mask irregularities that prevent a stable computation of the cross-power spectrum for multipoles $\ell > 500$; we thus consider only measurements at multipoles $\ell < 500$ at 3000 GHz.

³ <http://camb.info/>

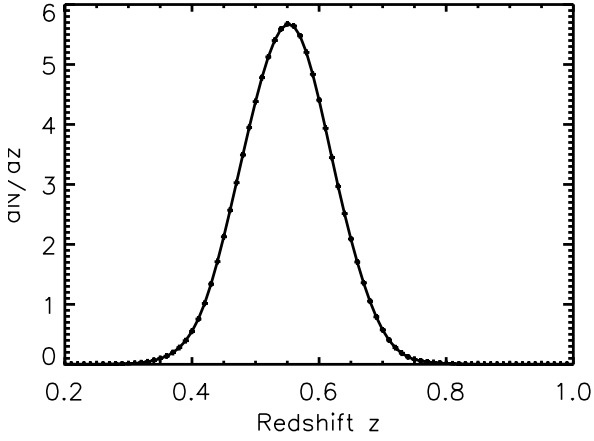


Fig. 2. Normalized SDSS-III DR8 LRG redshift distribution, peaked at $\bar{z} = 0.55$.

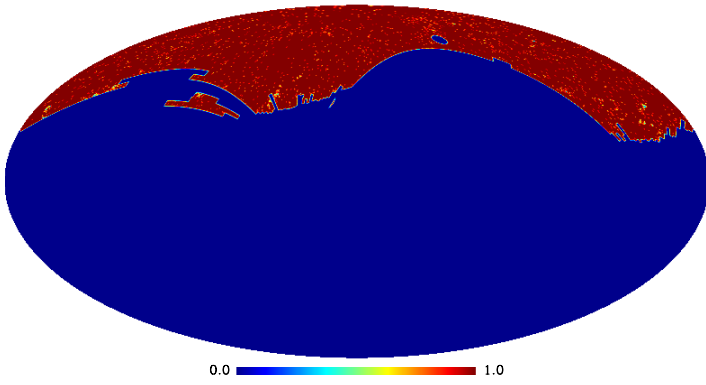


Fig. 3. Apodized mask used to cross-correlate the DR8 LRG map with the *Planck* temperature map at 857 GHz; the sky fraction unmasked is approximately $f_{sky} = 0.185$

We refer the reader to [Planck Collaboration VI \(2013\)](#); [Planck Collaboration VII \(2013\)](#); [Planck Collaboration VIII \(2013\)](#) for details related to the mapmaking pipeline, beam description and in general to the data processing for HFI data. In general, we used 2 masks to exclude regions with diffuse Galactic emission and extragalactic point sources respectively. The first mask accounts for diffuse Galactic emission as observed in the *Planck* data and leaves approximately 60% of the sky unmasked⁴. The second mask has been created using the *Planck* Catalogue of Compact Sources (PCCS, [Planck Collaboration XXVIII \(2013\)](#)) to identify point sources with signal-to-noise ratio greater or equal to 5 in the maps, and masking out a circular area of 3σ radius around each source (where $\sigma = FWHM/2.35$). The point sources to be removed have flux densities above a given threshold, as explained in [Planck Collaboration XXX \(2013\)](#). At 3000 GHz, we used a more aggressive mask which leaves 20% of the sky unmasked and covers more efficiently dust contaminated regions at high latitudes. The final footprint used in our cross-correlation analysis, which is simply the product of the LRG mask with each of the 4 CIB masks, has been smoothed with a gaussian beam with full width at half maximum of 10 arcminutes, to reduce possible power leakage; the mask used for the 857 GHz channel is shown in Fig. 3.

⁴ The mask can be found at http://pla.esac.esa.int/pla/aio/planckResults.jsp?withCATEGORY=MASK_gal-06

3. Cross-correlation measurement and analysis

We work in harmonic space, using *anafast* from the HEALPix package to cross-correlate temperature and density maps, and applying the pseudo- C_ℓ technique described in [Hivon et al. \(2002\)](#) to deconvolve both mask and beam from the cross-power spectrum.

A generic scalar field $\delta(\hat{n})$ can be expressed in terms of spherical harmonics $Y_{lm}(\hat{n})$ as:

$$\delta(\hat{n}) = \sum_{lm} a_{lm} Y_{lm}(\hat{n}), \quad (3)$$

where a_{lm} denotes the spherical harmonic coefficients:

$$a_{lm} = \int \delta(\hat{n}) Y_{lm}(\hat{n}) \quad (4)$$

and, for isotropic temperature and galaxy fields, it is possible to write their cross-power spectrum C_ℓ^{Tg} as:

$$\langle a_{\ell m}^T a_{\ell' m'}^g \rangle \equiv C_\ell^{Tg} \delta_{\ell\ell'}^K \delta_{mm'}^K, \quad (5)$$

where δ^K denotes the Kronecker delta function. In Fig. 4 we show the cross-power spectra measured for the four frequencies considered; error bars have been computed from Monte Carlo simulations and we refer the reader to Appendix A for details related to the pipeline employed in our measurement.

In order to test for possible contaminants in our datasets, we also performed two null tests. In the first one, we cross-correlate 500 CIB temperature random maps at 857 GHz (adding the expected level of foreground dust and instrumental noise) with the LRG map. The mean of the cross-correlation signal and its uncertainty are plotted in the left panel of Fig. 5; with a χ^2 of 6.7 for 9 degrees of freedom, our p-value is 0.67 and the null-test hypothesis of correlation consistent with zero is accepted.

We also performed a rotation test ([Sawangwit et al. 2010](#); [Giannantonio et al. 2012](#)), where one of the maps is rotated by an arbitrary angle and then cross-correlated with the other map: if the rotation angle $\Delta\phi$ is large enough and in absence of systematics, the resulting cross-power spectrum should be compatible with zero. Keeping fixed the CIB map, we computed $N = 89$ cross-power spectra with N galaxy maps, rotated by $\Delta\phi = 4$ degrees respect to each other and using the corresponding rotated galaxy masks; with $\chi^2 = 16.5$ for 9 degrees of freedom, we accept the null-test hypothesis of correlation consistent with zero.

Using the Limber approximation ([Limber 1953](#)), valid on all scales considered in our analysis, the theoretical cross-power spectrum at multipole ℓ and frequency ν can be written as:

$$C_\ell^{gT}(\nu) = \int \frac{dz}{\chi^2} \left(\frac{d\chi}{dz} \right)^{-1} b_{LRG} b_{CIB}(k, z) \frac{dN}{dz}(z) \frac{dS}{dz}(z, \nu) P_{dm}(k = \ell/\chi, z); \quad (6)$$

here $\chi(z)$ is the comoving angular diameter distance to redshift z , $P_{dm}(k, z)$ is the dark-matter power spectrum, while $b_{CIB}(k, z)$ and $\frac{dS}{dz}$ denote the bias of the CIB sources and the redshift distribution of their emissivity, respectively. In particular, the redshift distribution of CIB sources at the observed frequency ν is connected to the mean CIB emissivity per comoving unit volume $j_\nu(z)$ through the relation:

$$\frac{dS_\nu}{dz} = \frac{c}{H(z)(1+z)} \bar{j}_\nu(z), \quad (7)$$

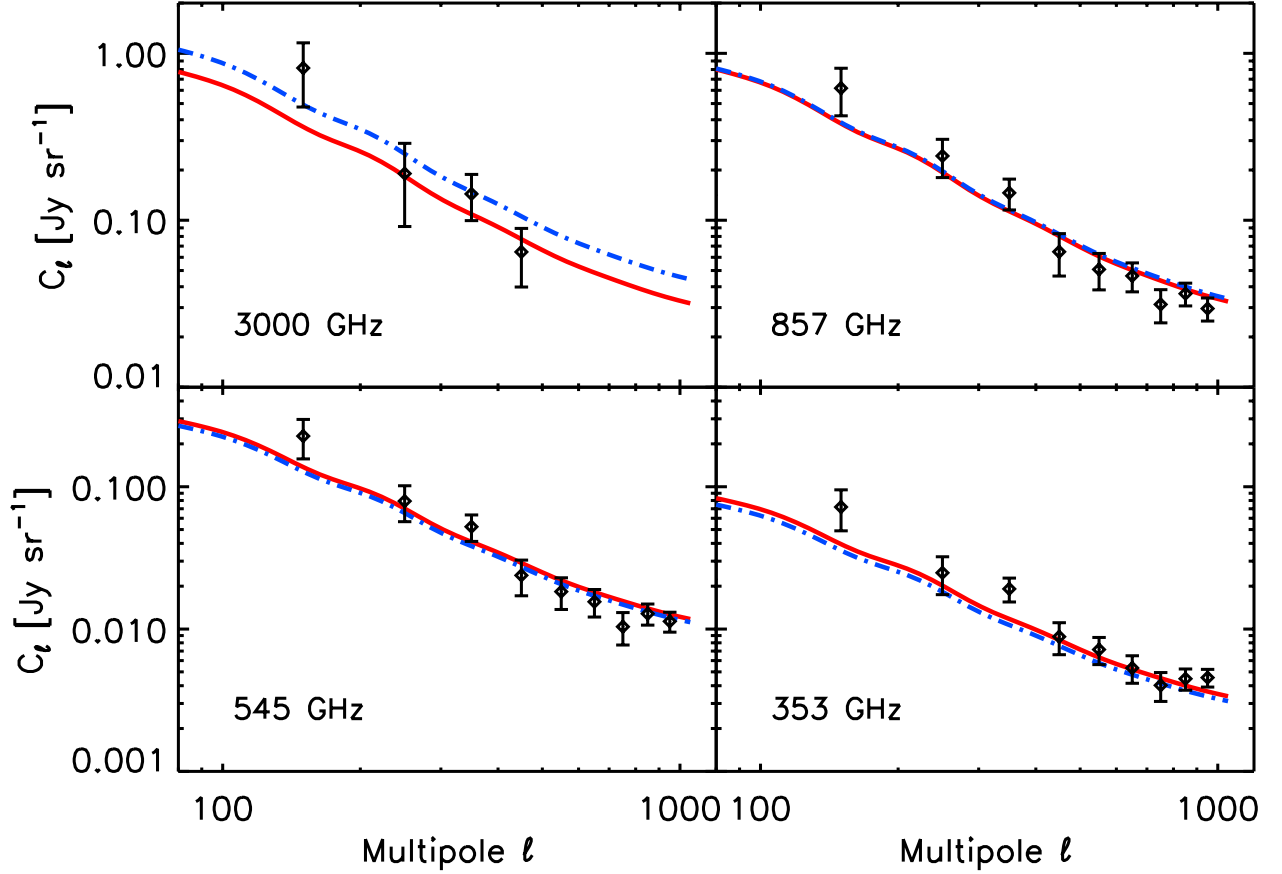


Fig. 4. Cross-power spectra measurements among CIB maps at 3000, 857, 545, and 353 GHz, and CMASS LRGs (black points); for the IRIS 3000 GHz channel we did not use data points at multipoles $l > 500$. Best-fit power spectra are shown for the parametric SED functional form (red lines) and for the effective SED (blue dashed-dotted lines).

where the galaxy emissivity $\bar{j}_\nu(z)$ can be written as

$$\bar{j}_\nu(z) = \int dL \frac{dn}{dL}(L, z) \frac{L_{(1+z)\nu}}{4\pi}; \quad (8)$$

here $L_{(1+z)\nu}$ and dn/dL denote the infrared galaxy luminosity and luminosity function respectively, while the term $(1+z)\nu$ denotes the rest-frame frequency. The emissivity $j_\nu(z)$ is modeled in the halo-model framework, using the extended halo-model approach introduced in [Shang et al. \(2012\)](#) and successfully applied in [Planck Collaboration XXX \(2013\)](#); we refer the reader to these papers for a detailed description of the theoretical motivations and limitations of the modeling used.

In this model, the galaxy infrared luminosity $L_{(1+z)\nu}$ is linked to the host dark-matter halo mass using the following parametric form:

$$L_{(1+z)\nu}(M, z) = L_0 \Phi(z) \Sigma(M) \Theta[(1+z)\nu]. \quad (9)$$

where the term L_0 is a normalization parameter that will be constrained with the CIB mean level at the frequencies considered. We will not further discuss this parameter in the rest of our analysis.

The term $\Phi(z)$ describes a redshift-dependent, global normalization, parameterized as:

$$\Phi(z) = (1+z)^{3.6} \quad (10)$$

where the power law exponent has been fixed to the mean value found in [Planck Collaboration XXX \(2013\)](#).

We also assume a log-normal function $\Sigma(M)$ for the dependence of the galaxy luminosity on halo mass:

$$\Sigma(M) = \frac{M}{(2\pi\sigma_{L/M}^2)^{1/2}} e^{-(\log_{10}(M) - \log_{10}(M_{\text{eff}}))^2 / 2\sigma_{L/M}^2}. \quad (11)$$

where M_{eff} describes the peak of the specific IR emissivity, and the parameter $\sigma_{L/M}$ describes the range of halo masses used for producing the IR luminosity; following [Shang et al. \(2012\)](#); [Planck Collaboration XXX \(2013\)](#), we assume the condition $\sigma_{L/M}^2 = 0.5$ while we fix the minimum halo mass at $M_{\text{min}} = 10^{10} M_\odot$ (compatible with [Viero et al. \(2013\)](#)) throughout this paper.

In general, a modified back-body functional form (see [Blain et al. 2003](#), and reference therein) can be assumed for galaxy SEDs:

$$\Theta(\nu, z) \propto \begin{cases} \nu^\beta B_\nu(T_d) & \nu < \nu_0; \\ \nu^{-\gamma} & \nu \geq \nu_0 \end{cases} \quad (12)$$

where B_ν denotes the Planck function, while the emissivity index β gives information about the physical nature of dust, in general depending on grain composition, temperature distribution of tunnelling states and wavelength-dependent excitation (e.g., [Meny et al. 2007](#)). The power-law function is used to temper the exponential (Wien) tail at high frequencies and obtain a shallower SED shape, more in agreement with observed SEDs (see

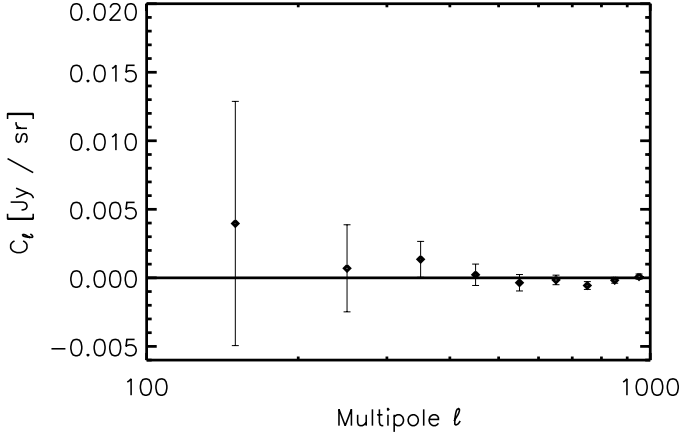


Fig. 5. Mean cross-power spectrum of 500 CIB random maps at 857 GHz with the LRG map; the signal is perfectly compatible with zero.

e.g. [Blain et al. \(2003\)](#)). The two SED functions at high and low frequencies are connected smoothly at the frequency ν_0 satisfying:

$$\frac{d \ln \Theta(\nu, z)}{d \ln \nu} = -\gamma. \quad (13)$$

We explicitly checked that our data do not allow to strongly constrain the emissivity index β and the SED parameter γ ; thus we fixed their values to the mean values found by [Planck Collaboration XXX \(2013\)](#), as $\beta = 1.7$ and $\gamma = 1.7$. Finally, the parameter T_d describes the average dust temperature of CIB sources at $z \sim 0.55$. Note that, since our measurement is restricted to quite a narrow redshift bin, we do not consider a possible redshift dependence of parameters such as M_{eff} or T_d ; the only redshift-dependent quantity is the global normalization term $\Phi(z)$.

The parameter space is sampled using a Monte Carlo Markov chain analysis with a modified version of the publicly available code CosmoMC ([Lewis & Bridle 2002](#)). We consider variations in the following set of three halo model parameters:

$$\mathcal{P} \equiv \{M_{\text{eff}}, T_d, L_0\}; \quad (14)$$

we assume the following priors on our physical parameters: $\log(M_{\text{eff}}) \in [11 : 13]M_\odot$ and $T_d \in [20 : 60]K$ and we explicitly checked that our results do not depend on the priors assumed.

Table 1. Mean values and marginalized 68% c.l. for halo model parameters

Parameter	Definition	Mean value
$\log(M_{\text{eff}})[M_\odot]$	Halo model most efficient mass	12.8 ± 0.15
$T_d [K]$	SED: dust temperature ($\bar{z}=0.55$)	26.0 ± 1.3

In addition to fitting to the four cross-power spectra, we also use the mean level of the CIB at 3000 GHz ($12.6^{+8.3}_{-1.7}$ nW m⁻²sr⁻¹), 857 GHz ($6.5^{+1.7}_{-1.6}$ nW m⁻²sr⁻¹) and 545 GHz ($2.1^{+0.7}_{-0.6}$ nW m⁻²sr⁻¹) deduced from galaxy number counts as useful priors to constrain the global normalization parameter L_0 .

Our set of three parameters allows us to obtain a very good fit to the data (Fig. 4), with a best-fit χ^2 of 26.9 for 31 degrees of freedom. Mean values and marginalized limits on the halo-model parameters considered here are given in Table 1. They are in good

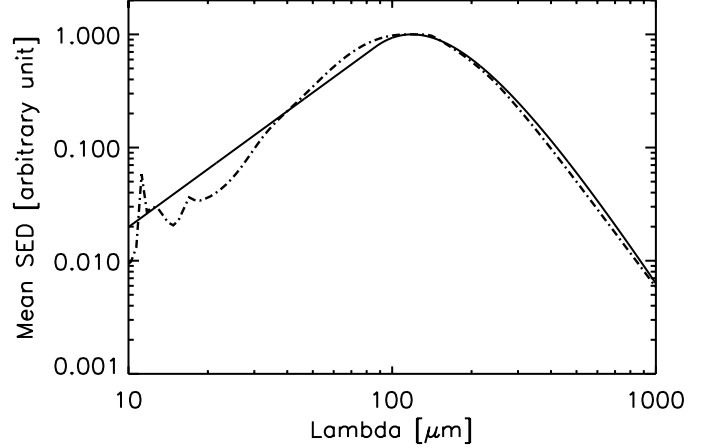


Fig. 6. Best-fit SEDs at $z = 0.55$ (both normalized to have amplitude equal to one at $\lambda=120 \mu\text{m}$) computed with the modified blackbody functional form (continuous line) and with the mean effective SED approach (dot-dash line), as in [Béthermin et al. \(2012\)](#).

agreement with results obtained from the analysis of *Planck* and IRIS auto-power spectra using the same parameterization for the CIB emissivity in [Planck Collaboration XXX 2013](#), providing a strong confirmation of their results. The mean value for the most efficient mass $\log(M_{\text{eff}}/M_\odot) = 12.8 \pm 0.15$ is somewhat larger than other recent analysis in literature ([Viero et al. 2013](#); [Shang et al. 2012](#); [Xia et al. 2012](#); [Planck Collaboration XXX 2013](#)) but in good agreement (at about 68% c.l.) with them. Using the values in Table 1, we also compute the approximate fraction of the total CIB responsible for the cross-correlation with LRGs, obtaining 11.8% at 3000 GHz, 3.9% at 857 GHz, 1.8% at 545 GHz and 1% at 353 GHz. Finally the mean values inferred for both the dust temperature ($T_d = 26.0 \pm 1.3$ K) and the bias ($b_{\text{CIB}} \sim 1.45$) are compatible with results obtained by [Planck Collaboration XXX \(2013\)](#) at $z \approx 0.55$.

In order to test the robustness of our results, we also replaced our parametric SED functional form with the mean effective SED $S_{\nu, \text{eff}}$ of all galaxies at redshift $z = 0.55$ from [Béthermin et al. \(2012\)](#), and we repeated the analysis, keeping only M_{eff} and L_0 as free parameters. With a χ^2_{red} of 1.0 (best-fit χ^2 equal to 31.9 for 32 degrees of freedom) our fit is satisfying; however, the most efficient halo mass at hosting star forming galaxies is $M_{\text{eff}} = 12.90 \pm 0.14$, higher than [Planck Collaboration XXX \(2013\)](#), and compatible at 95% c.l..

As we can see in Fig. 6, the parametric form used in this paper is similar to the mean effective SED for the range of wavelengths that matters in this analysis, giving a satisfactory confirmation of the goodness of our results. However, the γ parameter, which controls the high-frequency tail of the spectrum, fails to correctly reproduce the shape of real galaxy SEDs in the mid-infrared regime (from 10 to 30 μm), mainly because of broad line absorption from polycyclic aromatic hydrocarbon (PAH) molecules.

On linear scales, the cross-power spectra considered can also be fitted by power laws. Assuming a simple, two-parameter functional form such as:

$$C_l = A \left(\frac{l}{100} \right)^n, \quad (15)$$

it is possible to obtain a very good fit at all frequencies over the multipole range $100 < l < 500$. Mean values and marginalized

limits on the amplitudes A_ν and power-law slopes n_ν are provided in Table 2.

Table 2. Mean values and marginalized 68% c.l. for power-law parameters

Frequency	A	n
353	0.18 ± 0.07	-1.90 ± 0.36
545	0.60 ± 0.23	-2.08 ± 0.37
857	1.72 ± 0.65	-2.09 ± 0.36
3000	2.45 ± 1.33	-2.42 ± 0.57

4. Conclusions

We have measured the cross-correlation between LRGs from SDSS-III DR8 and CIB anisotropies from *Planck* and IRIS at 3000, 857, 545 and 353 GHz. Using an extended version of the halo model that connects galaxy luminosity to host halo mass with a simple parametric form, we confirmed the basic results obtained from recent analyses of CIB anisotropies, with a most efficient halo mass at hosting star forming galaxies with the value $\log(M_{\text{eff}}/M_\odot) = 12.84 \pm 0.15$ and mean dust temperature of CIB sources at $z \sim 0.55$ with the value $T_d = 26.0 \pm 1.3\text{K}$.

The cross-correlation of CIB sources with other tracers of the dark matter field from present and upcoming surveys will allow us to isolate the CIB signal in multiple redshift slices and thus constrain halo models parameters, CIB star formation and the bias between CIB sources and the external tracer as a function of redshift. These studies will be particularly interesting when performed with high-redshift sources (such as quasars), since current CIB model uncertainties are large for redshifts $z \gtrsim 2$.

However, a careful analysis of systematics is mandatory in order to exclude the possibility of correlated systematics between datasets; an example is stellar density affecting quasar catalogs and Galactic dust affecting CIB, which correlate and contaminate the cross-correlation signal. More generally, control of the effects of Galactic dust is critical to achieving a precise measurement of the cross-correlation, since it contributes significantly to the final error bar. Dust subtraction, using ancillary data and clean regions of the sky (as done in [Planck Collaboration XXX 2013](#)) can improve the signal-to-noise ratio, provided that large enough fields are considered.

Appendix A: Error bars computation

Our measurements are obtained as binned power spectra with a binning $\Delta_\ell = 100$, and we use a Monte Carlo approach to compute the uncertainty associated to each bin. In particular, we simulate $N = 500$ pairs of CIB temperature and LRG density maps, correlated as expected theoretically, adding the expected Poisson noise to both maps, in addition to an instrumental noise and a Galactic dust ‘noise’ term to the CIB frequency maps. More specifically, our pipeline for the computation of our error bars, also described in e.g., [Giannantonio et al. \(2008\)](#), works as follows:

- A simulated CIB frequency map is created (using the program *synfast* from the HEALPix package) as the sum of a clustering term plus three noise contributions due to shot-noise, Galactic dust contamination and instrument noise. The total power spectrum to be used as input in *synfast* can be

written as follows:

$$C_\ell(\nu) = C_\ell^{\text{TT,clust}}(\nu) + C_\ell^{\text{TT,SN}} + C_\ell^{\text{TT,dust}}(\nu) + N_\ell^{\text{instr}}(\nu) \quad (\text{A.1})$$

The clustering term for each frequency ν is simply computed using Eq. 6, and values for the shot-noise power spectrum $C_\ell^{\text{TT,SN}}$ are taken from Table 9 of [Planck Collaboration XXX \(2013\)](#). For the dust power spectrum we use a template taken as a power law $C_\ell^{\text{TT,dust}} \propto K l^\alpha$, where the amplitude K and the slope α are computed by fitting the measured dust-power spectrum from our CIB maps. Finally, the *Planck* instrument noise power spectrum $N_\ell^{\text{instr}}(\nu)$ is estimated from the jack-knife difference maps, using the first and second halves of each pointing period (see also [Planck Collaboration XXX \(2013\)](#)), while we refer to [Miville-Deschênes et al. \(2002\)](#) for the IRAS noise power spectrum computation.

- A galaxy map is also created as a sum of a clustering plus a shot-noise term:

$$C_\ell^{\text{gg}} = C_\ell^{\text{gg,clust}} + C_\ell^{\text{gg,SN}}. \quad (\text{A.2})$$

In the Limber approximation, the clustering term can be expressed as:

$$C_\ell^{\text{gg,clust}} = \int dz \frac{b_{\text{LRG}}^2}{\chi^2(z)} \left(\frac{dN}{dz}(z) \right)^2 P_{\text{dm}}(k = l/\chi(z), z), \quad (\text{A.3})$$

and the shot-noise power spectrum $C_\ell^{\text{gg,SN}}$ is directly estimated from the measured number of galaxies per pixel.

The galaxy map must be correlated with the CIB map. In general, two correlated galaxy-temperature maps are described by three power spectra, C_ℓ^{TT} , C_ℓ^{gg} and C_ℓ^{Tg} , where the last term is given by Eq. 6: It is easy to correlate a galaxy map with a given CIB map created with *synfast*. First we build a CIB map with a power spectrum $C_\ell^{\text{TT}}(\nu)$; then we make a second map with the same *synfast* seed used for the clustering term $C_\ell^{\text{TT,clust}}$ and with power spectrum $(C_\ell^{\text{Tg}})^2/C_\ell^{\text{TT}}$ and we add this second map to a third one made with a new seed and with power spectrum $C_\ell^{\text{TT}} - (C_\ell^{\text{Tg}})^2/C_\ell^{\text{TT}}$. These two maps will have amplitudes:

$$a_{\ell m}^{\text{TT}} = \xi_a (C_\ell^{\text{TT}})^{1/2} \quad (\text{A.4})$$

$$a_{\ell m}^{\text{gg}} = \xi_a C_\ell^{\text{Tg}} / (C_\ell^{\text{TT}})^{1/2} + \xi_b (C_\ell^{\text{gg}} - (C_\ell^{\text{Tg}})^2 / C_\ell^{\text{TT}})^{1/2},$$

where ξ denotes a random amplitude, which is a complex number with zero mean and unit variance ($\langle \xi \xi^* \rangle = 1$ and $\langle \xi \rangle = 0$). It is easy to see that, with these amplitudes, we have:

$$\langle a_{\ell m}^{\text{TT}} a_{\ell m}^{\text{TT}*} \rangle = C_\ell^{\text{TT}} \quad (\text{A.5})$$

$$\langle a_{\ell m}^{\text{TT}} a_{\ell m}^{\text{gg}*} \rangle = C_\ell^{\text{Tg}}$$

$$\langle a_{\ell m}^{\text{gg}} a_{\ell m}^{\text{gg}*} \rangle = C_\ell^{\text{gg}}$$

The maps obtained are then masked with the same mask as that used to analyze the real data, and the cross-power spectrum is then computed using the pseudo-power spectrum technique as in [Hivon et al. \(2002\)](#). The set of realizations of the cross-power spectrum provides the uncertainty on our estimate. The covariance matrix of the binned power spectrum C_b is:

$$C_{b,b'} = \langle (C_b - \langle C_b \rangle_{\text{MC}}) (C_{b'} - \langle C_{b'} \rangle_{\text{MC}}) \rangle_{\text{MC}} \quad (\text{A.6})$$

with $\langle \cdot \rangle$ standing for Monte Carlo averaging. The error bars on each binned C_b is:

$$\sigma_{C_b} = (C_{bb})^{1/2}. \quad (\text{A.7})$$

In order to test the stability of our results, error bars computed from simulations have been also confronted with an analytic estimate of the uncertainty:

$$\sigma_{C_b} = \left(\frac{1}{(2\ell + 1)\Delta l} \right)^{1/2} \left[(C_b^{Tg})^2 + (C_b^{gs})(C_b^{TT}) \right]^{1/2} \quad (\text{A.8})$$

where the term C_b^{TT} takes into account the power spectra related to CIB, Galactic dust, shot noise and instrument noise, as:

$$C_b^{TT} = C_b^{TT,CIB} + C_b^{\text{dust}} + C_b^{\text{SN}} + N_b^{\text{instr}}. \quad (\text{A.9})$$

For each bin, our Monte Carlo estimates of the uncertainties are within 10% of the uncertainties derived from Eq. A.8. In this regard, we decided to conservatively increase our error bars by 10% in the fitting process.

Acknowledgements. The development of *Planck* has been supported by: ESA; CNES and CNRS/INSU-IN2P3-INP (France); ASI, CNR, and INAF (Italy); NASA and DoE (USA); STFC and UKSA (UK); CSIC, MICINN and JA (Spain); Tekes, AoF and CSC (Finland); DLR and MPG (Germany); CSA (Canada); DTU Space (Denmark); SER/SSO (Switzerland); RCN (Norway); SFI (Ireland); FCT/MCTES (Portugal); and The development of *Planck* has been supported by: ESA; CNES and CNRS/INSU-IN2P3-INP (France); ASI, CNR, and INAF (Italy); NASA and DoE (USA); STFC and UKSA (UK); CSIC, MICINN and JA (Spain); Tekes, AoF and CSC (Finland); DLR and MPG (Germany); CSA (Canada); DTU Space (Denmark); SER/SSO (Switzerland); RCN (Norway); SFI (Ireland); FCT/MCTES (Portugal); and PRACE (EU).

A description of the Planck Collaboration and a list of its members, including the technical or scientific activities in which they have been involved, can be found at http://www.sciops.esa.int/index.php?project=planck&page=Planck_Collaboration.

P.S. would like to thank Alex Amblard for useful discussions. Part of the research described in this paper was carried out at the Jet Propulsion Laboratory, California Institute of Technology, under a contract with the National Aeronautics and Space Administration.

References

Amblard, A., Cooray, A., Serra, P., et al. 2011, *Nature*, 470, 510
 Béthermin, M., Daddi, E., Magdis, G., et al. 2012, *ApJ*, 757, L23
 Blain, A. W., Barnard, V. E., & Chapman, S. C. 2003, *MNRAS*, 338, 733
 Cooray, A. & Sheth, R. 2002, *Phys. Rep.*, 372, 1
 de Putter, R., Mena, O., Giusarma, E., et al. 2012, *ApJ*, 761, 12
 Dunkley, J., Hlozek, R., Sievers, J., et al. 2011, *ApJ*, 739, 52
 Eisenstein, D. J., Weinberg, D. H., Agol, E., et al. 2011, *AJ*, 142, 72
 Fixsen, D. J., Dwek, E., Mather, J. C., Bennett, C. L., & Shafer, R. A. 1998, *ApJ*, 508, 123
 Giannantonio, T., Crittenden, R., Nichol, R., & Ross, A. J. 2012, *MNRAS*, 426, 2581
 Giannantonio, T., Scranton, R., Crittenden, R. G., et al. 2008, *Phys. Rev. D*, 77, 123520
 Górski, K. M., Hivon, E., Banday, A. J., et al. 2005, *ApJ*, 622, 759
 Hall, N. R., Keisler, R., Knox, L., et al. 2010, *ApJ*, 718, 632
 Hauser, M. G., Arendt, R. G., Kelsall, T., et al. 1998, *ApJ*, 508, 25
 Hivon, E., Górski, K. M., Netterfield, C. B., et al. 2002, *ApJ*, 567, 2
 Ho, S., Cuesta, A., Seo, H.-J., et al. 2012, *ApJ*, 761, 14
 Lagache, G., Abergel, A., Boulanger, F., Désert, F. X., & Puget, J.-L. 1999, *A&A*, 344, 322
 Lagache, G., Bavouzet, N., Fernandez-Conde, N., et al. 2007, *ApJ*, 665, L89
 Lagache, G., Haffner, L. M., Reynolds, R. J., & Tufte, S. L. 2000, *A&A*, 354, 247
 Lewis, A. & Bridle, S. 2002, *Phys. Rev. D*, 66, 103511
 Limber, D. N. 1953, *ApJ*, 117, 134
 Ménard, B., Scranton, R., Schmidt, S., et al. 2013, *ArXiv e-prints*
 Meny, C., Gromov, V., Boudet, N., et al. 2007, *A&A*, 468, 171
 Miville-Deschênes, M.-A. & Lagache, G. 2005, *ApJS*, 157, 302
 Miville-Deschênes, M.-A., Lagache, G., & Puget, J.-L. 2002, *A&A*, 393, 749
 Navarro, J. F., Frenk, C. S., & White, S. D. M. 1997, *ApJ*, 490, 493
 Pâris, I., Petitjean, P., Aubourg, É., et al. 2013, *ArXiv e-prints*
 Planck Collaboration I. 2013, Submitted to *A&A*, [arXiv:astro-ph/1303.5062]
 Planck Collaboration VI. 2013, Submitted to *A&A*, [arXiv:astro-ph/1303.5067]
 Planck Collaboration VII. 2013, Submitted to *A&A*, [arXiv:astro-ph/1303.5068]
 Planck Collaboration VIII. 2013, Submitted to *A&A*, [arXiv:astro-ph/1303.5069]

Planck Collaboration XVI. 2013, Submitted to *A&A*, [arXiv:astro-ph/1303.5076]
 Planck Collaboration XVIII. 2011, *A&A*, 536, A18
 Planck Collaboration XVIII. 2013, Submitted to *A&A*, [arXiv:astro-ph/1303.5078]
 Planck Collaboration XXVIII. 2013, Submitted to *A&A*, [arXiv:astro-ph/1303.5088]
 Planck Collaboration XXX. 2013, Submitted to *A&A*, [arXiv:astro-ph/1309.0382]
 Puget, J.-L., Abergel, A., Bernard, J.-P., et al. 1996, *A&A*, 308, L5
 Reichardt, C. L., Shaw, L., Zahn, O., et al. 2012, *ApJ*, 755, 70
 Ross, A. J., Ho, S., Cuesta, A. J., et al. 2011, *MNRAS*, 417, 1350
 Sawangwit, U., Shanks, T., Cannon, R. D., et al. 2010, *MNRAS*, 402, 2228
 Shang, C., Haiman, Z., Knox, L., & Oh, S. P. 2012, *MNRAS*, 421, 2832
 Smith, R. E., Peacock, J. A., Jenkins, A., et al. 2003, *MNRAS*, 341, 1311
 Thomas, S. A., Abdalla, F. B., & Lahav, O. 2011, *MNRAS*, 412, 1669
 Tinker, J., Kravtsov, A. V., Klypin, A., et al. 2008, *ApJ*, 688, 709
 Tinker, J. L., Robertson, B. E., Kravtsov, A. V., et al. 2010, *ApJ*, 724, 878
 Viero, M. P., Ade, P. A. R., Bock, J. J., et al. 2009, *ApJ*, 707, 1766
 Viero, M. P., Wang, L., Zemcov, M., et al. 2013, *ApJ*, 772, 77
 White, M., Blanton, M., Bolton, A., et al. 2011, *ApJ*, 728, 126
 Wright, E. L., Eisenhardt, P. R. M., Mainzer, A. K., et al. 2010, *AJ*, 140, 1868
 Xia, J.-Q., Negrello, M., Lapi, A., et al. 2012, *MNRAS*, 422, 1324